

Available online at www.sciencedirect.com

### **ScienceDirect**

www.elsevier.com/locate/jes



www.jesc.ac.cn

# Simultaneous oxidation of Mn(II) and As(III) on cupric oxide (CuO) promotes As(III) removal at circumneutral pH

Lingqun Zeng<sup>1,3</sup>, Biao Wan<sup>2,4,\*</sup>, Qian Wang<sup>2</sup>, Yupeng Yan<sup>5</sup>, Yuanzhi Tang<sup>2</sup>, Xionghan Feng<sup>1</sup>

- <sup>1</sup>State Environmental Protection Key Laboratory of Soil Health and Green Remediation, College of Resources and Environment, Huazhong Agricultural University, Wuhan 430070, China
- <sup>2</sup> School of Earth and Atmospheric Sciences, Georgia Institute of Technology, Atlanta, GA 30332-0340, USA
- <sup>3</sup> Department of Environmental and Sustainable Engineering, University at Albany, SUNY, 1400 Washington Avenue, Albany, NY 12222, USA
- <sup>4</sup>Geomicrobiology, Center for Applied Geosciences, University of Tuebingen, 72076 Tuebingen, Germany.
- <sup>5</sup> Key Laboratory of Poyang Lake Watershed Agricultural Resources and Ecology of Jiangxi Province, College of Land Resources and Environment, Jiangxi Agricultural University, Nanchang 330045, China

### ARTICLE INFO

Article history:
Received 27 January 2022
Revised 17 March 2022
Accepted 17 March 2022
Available online 29 March 2022

Keywords:
Simultaneous oxidation
Mn(II)
As(III)
CuO
Metal oxides

#### ABSTRACT

Oxidation of Mn(II) or As(III) by molecular oxygen is slow at pH < 9, while they can be catalytically oxidized in the presence of oxide minerals and then removed from contaminated water. However, the reaction mechanisms on simultaneous oxidation of Mn(II) and As(III) on oxide mineral surface and their accompanied removal efficiency remain unclear. This study compared Mn(II) oxidation on four common metal oxides (y-Al<sub>2</sub>O<sub>3</sub>, CuO, \alpha-Fe<sub>2</sub>O<sub>3</sub> and ZnO) and investigated the simultaneous oxidation and removal of Mn(II) and As(III) through batch experiments and spectroscopic analyses. Among the tested oxides, CuO and \alpha-Fe2O3 possess greater catalytic activity toward Mn(II) oxidation. Oxidation and removal kinetics of Mn(II) and As(III) on CuO indicate that O2 is the terminal electron acceptor for Mn(II) and As(III) oxidation on CuO, and Mn(II) acts as an electron shuttle to promote As(III) oxidation and removal. The main oxidized product of Mn(II) on CuO is high-valent MnOx species. This newly formed Mn(III) or Mn(IV) phases promote As(III) oxidation on CuO at circumneutral pH 8 and is reduced to Mn(II), which may be then released into solution. This study provides new insights into metal oxide-catalyzed oxidation of pollutants Mn(II) and As(III) and suggests that CuO should be considered as an efficient material to remediate Mn(II) and As(III) contamination.

© 2022 The Research Center for Eco-Environmental Sciences, Chinese Academy of Sciences. Published by Elsevier B.V.

E-mail: biao.wan@uni-tuebingen.de (B. Wan).

<sup>\*</sup> Corresponding author.

### Introduction

In groundwater, arsenic (As) presents primarily as As(III) species (Katsoyiannis and Zouboulis, 2006; Ren et al., 2021). Generally, As(III) is more toxic and mobile than As(V) (Ferguson and Gavis, 1972; Coddington, 1986). Due to the high risk of As(III) to human health and the need to meet drinking water or wastewater discharge regulations, effective arsenic removal from wastewater and groundwater is highly desired and urgent. However, their removal and immobilization are challenging. For examples, As(III) oxidation and removal by  $\delta$ -MnO<sub>2</sub> into As(V) is reported to be an efficient strategy for As(III) remediation, while this reaction is limited by its weak adsorption capacity toward As(V) and the potential release of Mn(II) to solution at near neutral pHs (Manning et al., 2002).

In addition, manganese (II) (Mn(II)) is recently considered to be a potential pollutant in wastewater and might co-exist with As(III) (Schaefer et al., 2020). Environmental Mn(II) species could be oxidized through microbial and chemical oxidation processes (Bargar et al., 2005; Clement et al., 2009). Microbially mediated oxidation of Mn(II) is commonly considered as the most significant contributor to Mn oxide formation in natural environments (Webb et al., 2005; Butterfield et al., 2013). Surface-promoted oxidation of Mn(II) on environmental minerals also plays a critical role for Mn biogeochemical cycles in aquatic environments. Mn(II) oxidation can be accelerated in the presence of natural minerals, such as lepidocrocite ( $\gamma$ -FeOOH), goethite ( $\alpha$ -FeOOH), silica,  $\delta$ -A1<sub>2</sub>O<sub>3</sub> (Davies and Morgan, 1989), albite, hematite (Junta and Hochella Jr, 1994; Madden and Hochella Jr, 2005; Jung et al., 2021b), TiO<sub>2</sub> (Jung et al., 2021a) and ferrihydrite (Wang et al., 2015). Considering the reaction pathways of Mn(II) oxidation described above, it is desirable to find new materials that can promote As(III) oxidation and removal from the aqueous phase synergistically promoted by soluble Mn(II). These materials with the following potential properties are desirable: (1) high specific surface area (SSA) and point of zero charge (PZC), which are favorable for As(V) adsorption; (2) high catalytic activity toward Mn(II) oxidation to be high valent Mn components, which have strong As(III) oxidation ability at circumneutral pHs.

As one of the most popular *p*-type semiconducting oxides and engineered nanoparticles (Zhang *et al.*, 2014b), CuO nanoparticles are an excellent oxidation catalyst and adsorbent to remove As(III) from contaminated water due to their large SSA, high surface reactivity and PZC (Cao *et al.*, 2007; Martinson and Reddy, 2009; Yu *et al.*, 2012; McDonald *et al.*, 2015). However, our previous study showed that As(III) oxidation on CuO surface was pH-dependent and the oxidation rate was low at circumneutral pHs (Zeng *et al.*, 2018). This issue can be likely resolved with the presence of Mn oxides that could be formed from CuO-catalyzed Mn(II) oxidation. However, the reactions in the CuO, Mn(II) and As(III) ternary system at environmentally relevant pHs await characterization.

To reveal the reaction mechanisms of simultaneous Mn(II) and As(III) oxidation, we designed the oxidation experiments under various concentrations of initial Mn(II) close to natural environments to compare Mn(II) oxidation by a variety of common metal oxides ( $\gamma$ -Al<sub>2</sub>O<sub>3</sub>, CuO,  $\alpha$ -Fe<sub>2</sub>O<sub>3</sub> and ZnO). The kinetics of As(III) oxidation in the presence and absence of

Mn(II) at circumneutral pH 8 were studied using wet chemistry methods. Then, Mn(II) oxidized intermediate products and As(III) oxidized final products were characterized by multiple spectroscopic techniques, such as X-ray photoelectron spectroscopy (XPS) and X-ray adsorption spectroscopy (XAS). Finally, based on these result analyses, we proposed the potential mechanisms of Mn(II) and As(III) simultaneous oxidation on CuO surface and figured out how the process promotes the removal of these two pollutants at the same time.

#### 1. Materials and methods

#### 1.1. Materials

CuO synthesis procedure and characterization results can be found in our previous study (Zeng et al., 2018). Preparation, source, and characterizations of  $\alpha$ -Fe<sub>2</sub>O<sub>3</sub>,  $\gamma$ -Al<sub>2</sub>O<sub>3</sub> and ZnO are provided in Appendix A Text S1 and Table S1. All other chemicals used in this study are analytical grades.

### 1.2. Mn(II) oxidation and removal by four metal oxides at different pH values

Batch experiments were conducted in glass conical flasks (volume 150 mL) by the mixture of 0.1 g CuO,  $\alpha$ -Fe<sub>2</sub>O<sub>3</sub>,  $\gamma$ -Al<sub>2</sub>O<sub>3</sub> or ZnO with 100 mL of fresh 0.78 mmol/L Mn(II). The background electrolyte was 0.01 mol/L NaCl. The suspensions were agitated by magnetic stirring at 10 Hz. To investigate the effect of solution pHs on Mn(II) adsorption and oxidation on different metal oxides, automatic titrator (Metrohm 907, Titrando, Switzerland) was applied to maintain/adjust pH values of the reaction suspensions automatically by adding 0.1 mol/L NaOH or HCl. The experiments were conducted in an open system, allowing atmospheric O2 diffusion into reaction suspensions. After 24 hr reaction, 5 mL aliquot of the suspension was taken and immediately filtered through 0.22- $\mu m$  Millipore membrane syringe filter to get the supernatants for dissolved Mn(II) measurement/Mn(II) removal determination. The specific kinetics of Mn(II) adsorption and oxidation are performed for CuO and  $\alpha$ -Fe<sub>2</sub>O<sub>3</sub> at pH 8. Particularly, catalytic oxidation and adsorption kinetics of Mn(II) were conducted by adding 0.2 g CuO and  $\alpha\text{-Fe}_2\text{O}_3$  into 200 mL of 0.01 mol/L NaCl and 0.78 mmol/L Mn(II) solution. Mn(II) removal experiments were performed without the repeat treatment due to the usage of automatic titrator in these experiments. The concentration of dissolved Mn(II) in the supernatants was measured by atomic absorption spectrometry (AAS) (Varian AAS 240FS, US). Leucoberbelin blue I (LBB) colorimetric assay was applied to determine the Mn oxidation equivalent percentage (Zhu et al., 2017). Oxidation equivalent percentage can be used to quantify the Mn(II) oxidation rate, which was determined by the LBB colorimetric assay. For example, 100% oxidation rate represents that Mn(II) was completely oxidized to Mn(IV).

### 1.3. Kinetics of simultaneous As(III) and Mn(II) oxidation on $\mbox{CuO}$

Adsorption-oxidation kinetics were conducted by reacting 0.2 g CuO with 200 mL of 10 mg/L As (III) in the presence of 0.78

mmol/L Mn(II) at pH 8. The background electrolyte is NaCl with the concentration of 0.01 mol/L. The suspensions were agitated by magnetic stirring at 10 Hz over 24 hr reaction time. pH values of the batch experiments were measured using a pH meter (FE20, Mettler-Toledo). The solution pH was manually adjusted to and maintained at desired pH values  $\pm$  0.1 using 0.1 mol/L HCl and NaOH. At selected time points, 5 mL aliquot of the suspension was taken and immediately filtered through 0.22-µm Millipore membrane syringe filter to analyze the concentration of As(III) and As(V) in supernatants. The wet solids on the membrane were dissolved by 1 mL of 1 mol/L HCl to analyze the amount of As(III) and As(V) adsorbed onto the CuO surface. Another 5 mL suspension was directly dissolved by 1 mL of 1 mol/L HCl to analyze the total amount of As(III) and As(V) in the suspensions. All experiments were conducted in triplicates. Control experiments were conducted in the absence of Mn(II). The concentration of As(III) and As(V) in solution or on CuO surface were tested based on our previous report (Zeng et al., 2018). The concentration of dissolved Mn(II) in the supernatants and Mn oxidation percentage were analyzed with the same procedures as described in the Section 1.2.

### 1.4. As(III) adsorption and oxidation at different Mn(II)/As(III) molar ratios

The experiments were carried out in 100 mL conical flask by mixing 0.1 g CuO with 100 mL of 0.01 mol/L NaCl containing fresh As(III) and Mn(II). To investigate the effect of Mn(II)/As(III) molar ratios on As(III) adsorption and oxidation on CuO surface, 100 mL of 0.01 mol/L NaCl solution contained a fixed 10 mg/L As(III) and was added by variable volumes of 5 mmol/L MnCl $_2$  stock solution to achieve Mn(II) concentrations of 0, 0.065, 0.13, 0.26, 0.52, 0.78, 1.3, and 2.6 mmol/L, which can make Mn(II)/As(III) ratios to be 0, 0.5, 1, 2, 4, 6, 10, and 20. All experimental procedures on concentrations of As and Mn determination were the same with the previous descriptions in Sections 1.2-1.3.

### 1.5. X-ray photoelectron spectroscopy analysis

To determine the oxidation state of As and Mn during the reaction process, the samples prepared by reacting 0.05 g CuO with 50 mL of 10 mg/L As(III) and 0.78 mmol/L Mn(II) (Mn(II)/As(III) ratio = 6) for 0.5, 2, 6, and 12 hr were measured using the XPS spectrometer (VG multilab 2000 equipment Thermo scientific, East Grinstead, West Sussex, UK) with a monochromatic Al K $\alpha$  X-ray source. The solid samples at each interval were centrifuged and rinsed with DI water for twice, immediately. Then, the centrifuged solids were freeze-dried for further XPS analysis. The scans were carried out in an energy range of 5–1100 eV for C 1s, Mn 2p, and As 3d XPS spectra. The position of binding energy was corrected by fixing the C 1s peak at 284.6 eV using the Advantage v6.5 software.

### 1.6. Mn and As K-edge X-ray absorption spectroscopy

Mn and As K-edge XAS was used to in situ investigate the alteration of Mn and As oxidation states as reaction time increased. The experimental procedures employed were similar

to the reported method (Ginder-Vogel et al., 2009), and are described as follows. The Mn and As K-edge XAS spectra were collected at ~25°C in the 1W1B beamline at the Beijing Synchrotron Radiation Facility (BSRF) in fluorescence mode. Based on the detection limits (≥100 mg/L for As) of Lytle prober, the concentrations of Mn(II) (10 mmol/L) and CuO (5 g/L) has been increased for in situ Mn and As K edge XAS measurements. The reaction was performed in 50-mL polypropylene reaction vessels. At time intervals of 2 hr, 24 hr and 48 hr, 5 mL aliquot of the suspension was taken and immediately sealed to a circular hole of 1 cm radius within the center of a 3 cm  $\times$  3 cm glass plate with Kapton tape, backed with Kapton film to prevent the interaction between the tape and suspension. Upon the commencement of the oxidation reaction, the Mn K-edge XAS or As K-edge XAS spectra were immediately collected between 6.35 and 7.2 keV and between 11.85 and 11.95 keV, respectively. The measurement time for each spectrum of Mn or As XAS was approximately 15 min. The Athena program was used for background removal and linear combination fittings (LCF) to quantify the speciation variations for Mn speciation (Ginder-Vogel et al., 2009).

#### 2. Results

### 2.1. Mn(II) oxidation and removal by different metal oxides

The total percentages of aqueous Mn(II) oxidation and removal after 12 hr at different pHs were investigated to explore the effects of solution pHs on Mn(II) oxidation and removal on CuO,  $\alpha$ -Fe<sub>2</sub>O<sub>3</sub>,  $\gamma$ -Al<sub>2</sub>O<sub>3</sub>, and ZnO surface (Fig. 1). The removal percentages of Mn(II) from the solution in the presence of CuO,  $\alpha$ -Fe<sub>2</sub>O<sub>3</sub>,  $\gamma$ -Al<sub>2</sub>O<sub>3</sub>, and ZnO are showed in Fig. 1a and four tested metal oxides display the different reactivity for Mn(II) removal at various pH values. The removal percentages of Mn(II) from the solution have a positive relationship to the oxidation equivalent percentages of Mn(II) on four different metal oxides, indicating that the removal of aqueous Mn(II) is highly associated with the catalytic oxidation of Mn(II) by these metal oxides. Surface adsorption of Mn(II) on oxide minerals or bulk/surface Mn(OH)<sub>2</sub> precipitation are two additional factors to facilitate Mn(II) removal as high removal percentages are observed in the absence of metal oxide and the presence ZnO and  $\gamma$ -Al<sub>2</sub>O<sub>3</sub> (Fig. 1a), which show a low ability of Mn(II) oxidation when pH is below 9 (Fig. 1b). As expected, chemical auto-oxidation of Mn(II) only occurred at pH above 7 (Emerson, 2000), while Mn(II) oxidation is significantly enhanced in the presence of oxides as pH increases from 7 to 9 (Fig. 1b). When pH values are below 7, Mn(II) oxidation is limited even in the presence of 1 g/L metal oxides. At pH 7, the slight oxidation of Mn(II) is observed in the presence of CuO and α-Fe<sub>2</sub>O<sub>3</sub> with Mn(II) oxidation percentages of 17% and 16%, respectively. Mn(II) oxidation percentages jump to 82% and 78% in the presence of CuO and  $\alpha$ -Fe<sub>2</sub>O<sub>3</sub> at pH 8, which are obviously higher than ZnO and  $\gamma$ -Al<sub>2</sub>O<sub>3</sub>.

The kinetics of aqueous Mn(II) removal percentages at pH 8 in the absence and presence of CuO and  $\alpha$ -Fe<sub>2</sub>O<sub>3</sub> are compared (Fig. 2a).  $\alpha$ -Fe<sub>2</sub>O<sub>3</sub> displays a good ability of Mn(II) removal from the solution and can completely remove Mn(II) within 5 hr.

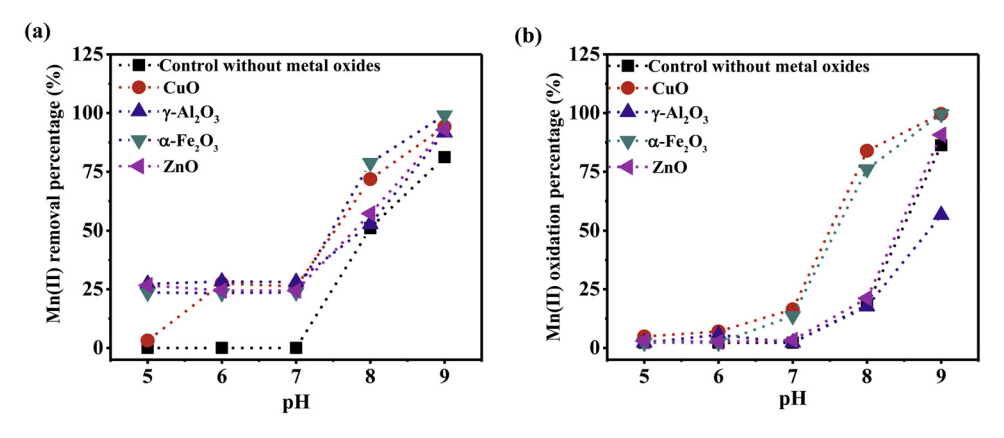


Fig. 1 – The removal percentages of aqueous Mn(II) (a) and oxidation equivalent percentages of Mn(II) (b) by four different metal oxides at different solution pHs. The initial [Mn(II)] = 0.78 mmol/L; [Metal oxides] = 1.0 g/L.

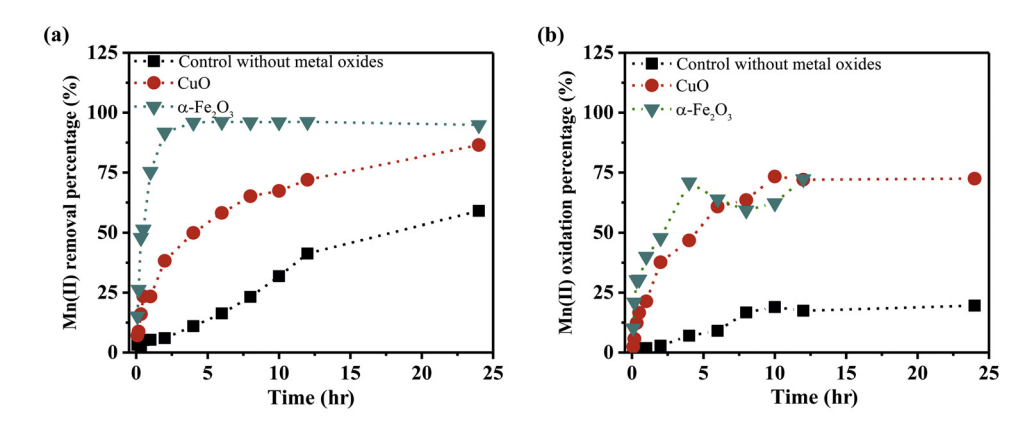


Fig. 2 – Kinetics of aqueous Mn(II) removal (a) and Mn(II) oxidation (b) in the presence of CuO and  $\alpha$ -Fe<sub>2</sub>O<sub>3</sub> at pH 8. The initial [Mn(II)] = 0.78 mmol/L; [Metal oxides] = 1.0 g/L.

However, over a total 24 hr reaction period, the removal ability of Mn(II) by CuO is close to  $\alpha$ -Fe<sub>2</sub>O<sub>3</sub>. The dynamics and kinetics of Mn(II) oxidation by CuO and  $\alpha$ -Fe<sub>2</sub>O<sub>3</sub> at pH 8 are shown in Fig. 2b. In the presence of CuO and  $\alpha$ -Fe<sub>2</sub>O<sub>3</sub>, Mn(II) oxidation occurs rapidly over 24 hr reaction. Mn(II) oxidation percentage increases with the increasing reaction time in the presence of either CuO or  $\alpha$ -Fe<sub>2</sub>O<sub>3</sub> and eventually reaches the equilibrium steady to  $\sim$ 75% after 5 hr for  $\alpha$ -Fe<sub>2</sub>O<sub>3</sub> and 12 hr for CuO (Fig. 2b), respectively. As a comparison, auto-oxidation of Mn(II) at pH 8 reaches equilibrium steady after 12 hr and with Mn oxidation percentage of only 20%. Meanwhile, in the presence of CuO, Mn(II) oxidation is limited under N<sub>2</sub> condition and high under air or O<sub>2</sub> conditions (Appendix A Fig. S1). The oxidation extent can reach to  $\sim$ 90% with the pumping of O<sub>2</sub>, implying that O<sub>2</sub> plays a crucial role to be electron acceptors for Mn(II) oxidation

To quantitatively compare the oxidation rates of Mn(II) in the presence CuO and  $\alpha\text{-Fe}_2O_3$ , the proportion of Mn(II) oxidation over time at pH 8 is fitted using a first-order kinetic equation. The fitted kinetic rate constants are 0.110 and 0.1993  $hr^{-1}$  for CuO and  $\alpha\text{-Fe}_2O_3$ , respectively, which are an order of magnitude higher than Mn(II) auto-oxidation rate of 0.0156  $hr^{-1}$  in the absence of metal oxides (Appendix A Table S2). These re-

sults indicate that both CuO and  $\alpha\text{-Fe}_2O_3$  have strong catalytic reactivity toward Mn(II) oxidation.

### 2.2. Roles of aqueous Mn(II) in As(III) adsorption and oxidation

To investigate the effects of aqueous Mn(II) on As(III) adsorption and oxidation on CuO surface, As(III) adsorption and oxidation experiments were performed under same initial As(III) concentration and different ratios of Mn(II)/As(III) at pH 8. Control experiments were conducted in the absence of aqueous Mn(II) (i.e., Mn(II)/As(III) ratio = 0). The distributions of As(III) and As(V) on CuO surface and in solution at different initial Mn(II) concentrations after 24 hr reaction are shown in Fig. 3. The total amounts of oxidized As(III) increase with the increase of Mn(II) loadings. The oxidation percentage of As(III) to As(V) are 33.2%, 44.9%, 54.3%, 66.7 % and 81.2 % as Mn(II)/As(III) ratios increase from 0 to 0.5, 1, 2 and 4, respectively. When Mn(II)/As(III) ratios further increase to 6, 10 and 20, the oxidation of As(III) to As(V) is stable at approximate 85.0% without the further increase. Therefore, the amounts of As(III) oxidation is promoted due to the Mn(II) addition and the As(III) oxidation rates increase with the increase of Mn(II)/As(III) ratios. The optimal oxidation rate could be achieved at the Mn(II)/As(III) ratio of 6. Under this condition,

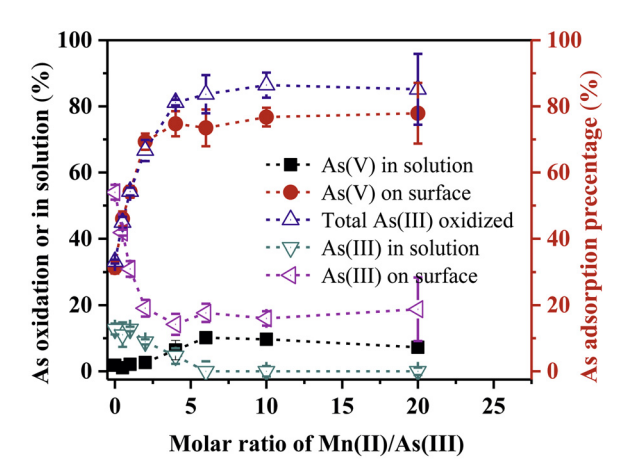


Fig. 3 – Effect of Mn(II)/As(III) molar ratios (0-20) on the catalytic oxidation of As(III) by CuO at pH 8. The initial [Mn(II)] ranges from 0-2.6 mmol/L. [Metal oxides] and [As(III)] are fixed to 1.0 g/L and 10 mg/L, respectively.

As(V) produced from As(III) oxidation is mainly sequestrated on CuO surface. Solution As(V) and As(III) concentrations decrease by approximate 92% with initial As(III) at 10 mg/L in the experiment. Meanwhile, at pH 8, the extents of Mn(II) oxidation on CuO accompanying with As(III) oxidation remarkably increase at low Mn(II)/As(III) molar ratios and reach to the steady state when Mn(II)/As(III) molar ratios are beyond 6 (Appendix A Fig. S3). These results indicates that the addition of aqueous Mn(II) can significantly promote As(III) oxidation and As(V) adsorption/total As removal; and the ratios between Mn(II) and As(III) is important for As(III) removal.

### 2.3. Kinetics of As(III) adsorption and oxidation in present of Mn(II)

The dynamics of As(III) and As(V) speciation distributions in solution or on CuO surface are shown in Fig. 4. At the first 2 hr reaction, As(III) adsorption is rapid regardless of the presence or absence of Mn(II). The adsorption amounts of As(III) reached to 60% and 50% at 2 hr in the absence and presence of Mn(II), respectively. The adsorption amounts of As(III) in the presence of Mn(II) was a little lower than that in absence of Mn(II) at this early stage probably since Mn(II) adsorption on CuO surface leads to the occupation of some surface As(III) adsorption sites. As the reaction proceeds, the amounts of As(III) on CuO surface in the absence and presence of Mn(II) changed significantly. In the absence of Mn(II), the amount of As(III) on CuO surface is stable at  $\sim$  65% as the reaction time increases from 2 hr to 24 hr. However, in the presence of Mn(II), the amount of As(III) on CuO surface decreases obviously from 50% at 2 hr to 8% at 24 hr. It is thus concluded that the As(III) oxidation amounts in the presence of Mn(II) are higher than that in the absence of Mn(II) at each tested time point (Fig. 4a).

Accompanying with As(III) oxidation, soluble Mn(II) decreases as reaction time increases in the ternary system of CuO-Mn(II)-As(III) at Mn/As ratio of 6 and pH 8 (Fig. 4d). After 24 hr of reaction, 62% of Mn are soluble in solution as Mn(II) form and 38% of Mn is fixed on CuO surface probably as high-

valent MnO $_{\rm X}$  phases. The recent studies found that abiotic oxidation of aqueous Mn(II) in the presence of natural oxide minerals led to the heterogeneous nucleation of romanechite-like (2 × 3 tunnel structure) Mn oxide on  $\alpha$ -Fe $_2$ O $_3$  and todorokite-(3 × 3 tunnel structure) and romanechite-like Mn oxides on TiO $_2$  under circumneutral conditions (Jung et al., 2021a; Jung et al., 2021b). In this study, O $_2$  cannot directly and efficiently oxidize As(III) (Appendix A Fig. S2), consistent with the previous study (Bissen and Frimmel, 2003), while O $_2$  has a potential ability to oxidize Mn(II) into MnO $_{\rm X}$  under our experimental conditions (Fig. 1). The newly formed MnO $_{\rm X}$  phases might contain both Mn(III) and Mn(IV) species, which have strong ability to oxidize As(III) into As(V) (Lan et al., 2018). The 38% high-valent Mn phases on CuO surface are still remaining even after complete As(III) oxidation.

To further obtain the apparent kinetic rates of As(III) oxidation by CuO in the absence and presence of Mn(II) at pH 8, the As(III) concentration in the suspensions is fitted by a first-order kinetic equation. The fitted kinetic rate constants are 0.0087 and 0.11 hr $^{-1}$  in the absence and presence of Mn(II), respectively (Table 1). The oxidation rate of As(III) in the presence of Mn(II) is about 12 times higher than in the absence of Mn(II), indicating that Mn(II) significantly promotes the oxidation rate of As(III) on CuO surface.

In addition, the oxidation kinetics of As(III) under pure  $N_2$  and  $O_2$  atmospheres in the presence of Mn(II) and CuO at pH 8 are determined to investigate the impact of  $O_2$  on As(III) oxidation. The oxidation rate constant of As(III) is low around 0.042 hr $^{-1}$  under  $N_2$  condition (Appendix A Fig. S4 and Table 1), while the pumping of pure  $O_2$  increases the oxidation rate constant (0.21 hr $^{-1}$ ) which is greater than that in air (0.12 hr $^{-1}$ ), suggesting that  $O_2$  is the final electron acceptor for As(III) oxidation and its presence accelerates catalyzed oxidation of both Mn(II) and As(III) by CuO at pH 8 in the CuO, Mn(II) and As(III) ternary system. The difference of As(III) oxidation rate constant in air (21%  $O_2$ ) and pure  $O_2$  (100%  $O_2$ ) conditions is attributed to the different concentrations of  $O_2$  in the gas.

## 2.4. X-ray absorption and X-ray photoelectron spectroscopy

In situ XAS was conducted to directly monitor the oxidation products of Mn(II) and As(III) on CuO surface. To obtain an optimal signal-to-noise ratio, we increased the concentrations of initial Mn(II) for the in situ Mn and As K-edge XAS measurements than those in batch experiments. The linear combination fitting (LCF) based on a database of standard (17 references) spectra is used for the Mn valence fitting (Manceau et al., 2012). The in situ Mn K-edge XANES spectra are collected as a function of time and the fitting results are shown in Fig. 5a and Table 2 in the CuO and Mn(II) binary system.

In the CuO and Mn(II) binary system, in situ XAS spectra indicate that Mn(II) is oxidized to high valence Mn by CuO after 48 hr at pH 8 (Fig. 5a), consistent with the results of batch experiments (Fig. 2b). As reaction proceeds, Mn(II) is gradually oxidized to Mn(III) and Mn(IV). The relative percentages of Mn(II), Mn(III) and Mn(IV) after 2 hr reaction are 89.00%, 10.70%, and 0.00%, respectively. After 24 hr reaction, Mn(III) percentage increases to 74.9% at 24 hr that is beyond the percentages of Mn(II) and Mn(IV) and then keeps stable.

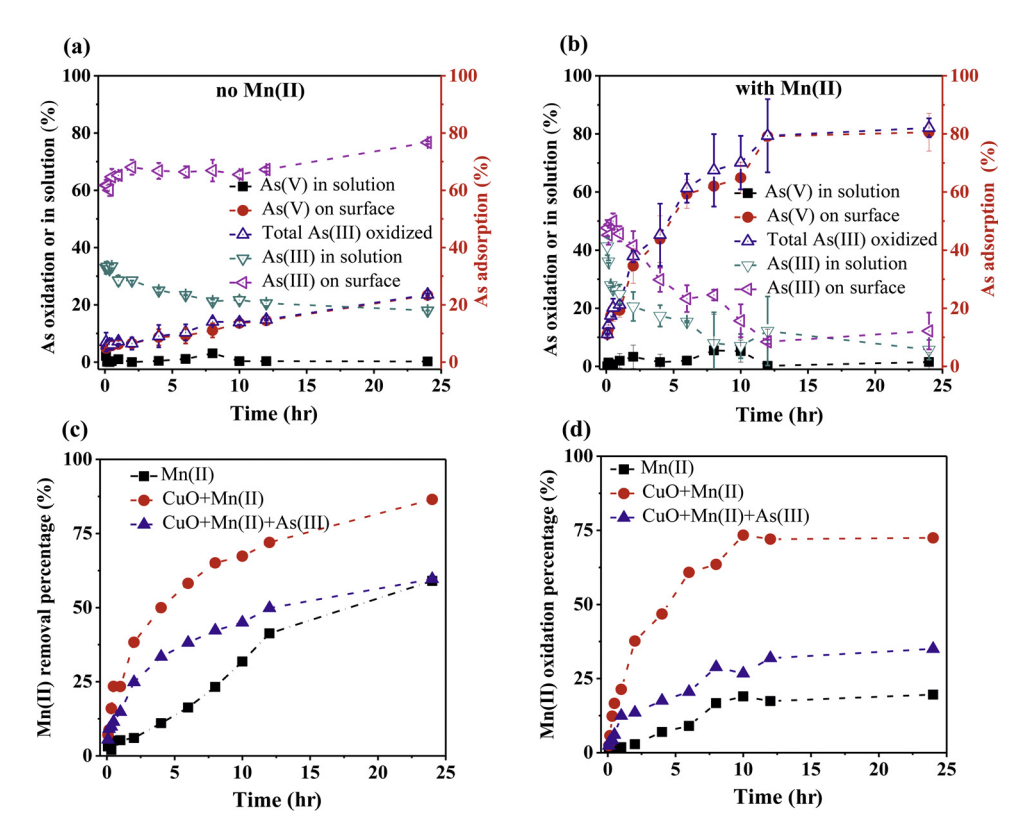


Fig. 4 – Kinetics of As(III) oxidation and phase partition of As(III) and As(V) at pH 8 in the absence of Mn(II) (a) and in the presence of 0.78 mmol/L Mn(II) (i.e., Mn/As=6) (b); and the accompanied Mn(II) removal from the solution (c) and Mn(II) oxidation percentages (d) at pH 8 in the presence of As(III) under air condition. [CuO] = 1.0 g/L.

Table 1 – Apparent first-order rate constants of As(III) oxidation on CuO surface in the absence and presence of Mn(II) at pH 8.							
System	Reaction atmosphere	Reaction time (hr)	Number of data points for fitting	k (hr <sup>-1</sup> )	R <sup>2</sup>		
CuO and As(III)	Air	12	11	0.0087	0.9811		
CuO, Mn(II) and As(III)	N <sub>2</sub> Air O <sub>2</sub>	9 12 12	8 11 11	0.0421 0.1166 0.2095	0.8744 0.9863 0.9924		
The rate constants of		<del></del>	11				

The rate constants of As(III) removal were determined by linear regression analysis of the noted time-periods for the plots in Fig. 4 and Appendix A Fig. S4.

Table 2 – LCF fitting results of Mn K-edge XAS spectra shown in Fig. 5.								
System	Reaction time (hr)	Percentage (%)						
		Mn(II)	Mn(III)	Mn(IV)				
CuO and Mn(II)	2	89.0	10.7	0.0				
	24	9.9	74.9	15.0				
	48	6.0	70.0	24.0				
CuO, Mn(II), and As(III)	2	77.0	23.0	0.0				
	24	49.0	25.0	26.0				
	48	25.0	65.0	10.0				

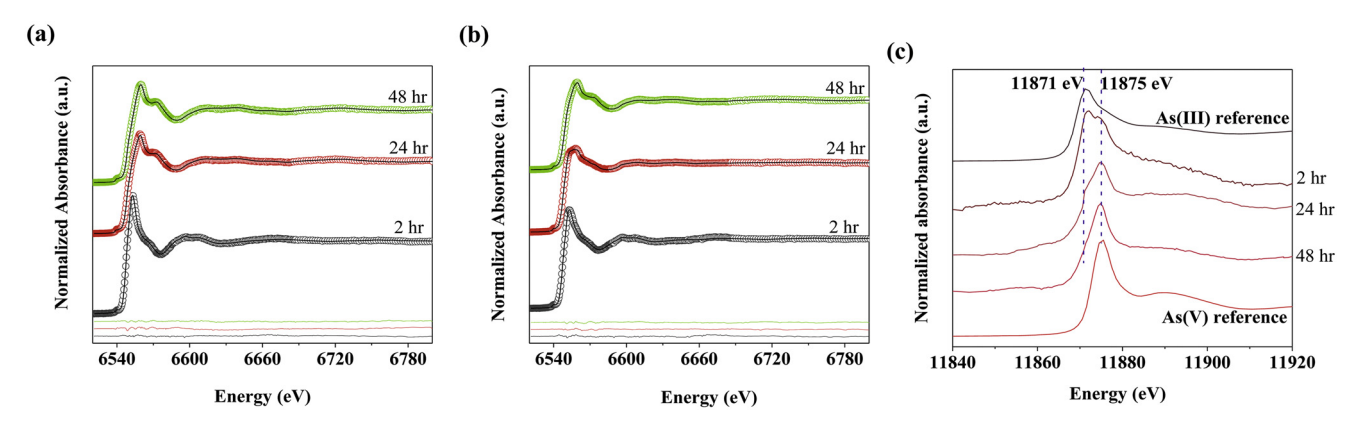


Fig. 5 – Mn K-edge XANES spectra of Mn(II) oxidation samples in the absence of As(III) (a) and in the presence of As(III) (b). Empty cycles and solid lines represent the raw data and linear combination fitting (LCF) results, respectively. The fitting parameters are shown in Table 2. (c) As K-edge XANES spectra of As(III) oxidation on CuO in the presence of Mn(II) at different reaction time. As K-edge XAS spectra of 6.67 mmol/L Na<sub>3</sub>AsO<sub>3</sub> (As(III)) and 6.67 mmol/L Na<sub>3</sub>AsO<sub>4</sub> (As(V)) solutions are used as As(III) and AS(III) standard references, respectively.

In the CuO, Mn(II) and As(III) ternary system, the percentages of the produced Mn(III) and Mn(IV) species are different at various reaction times. Most of the Mn(II) transformed to both Mn(III) (65%) and Mn(IV) (10%) within the reaction time (Fig. 5b). Meanwhile, As K-edge XAS was conducted to directly monitor the oxidation of As(III) in the presence of CuO and Mn(II) at pH 8. The energy peaks in in situ As XANES spectra gradually shift from 11871 to 11875 eV over 48 h (Fig. 5c), implying that As(III) is oxidized to As(V) by CuO in the presence of Mn(II) at pH 8, consistent with the results of batch experiments (Fig. 4b). As the reaction time increases, As(III) is gradually oxidized to As(V) and As(III) is completely oxidized after 48 hr reaction since the spectrum at this time is well matched with that of As(V) standard compounds (Fig. 5c).

Mn 2p XPS spectra and fit results of the solid products after the reaction in the presence of As(III) at different reaction times are collected and shown in Fig. 6. The fitting coefficients and different peak areas of XPS spectra are summarized in Appendix A Table S3. The binding energy of Mn(II), Mn(III) and Mn(IV) is cited from the reported method (Yin et al., 2013). The binding energy of Mn with low oxidation state is located on the low-energy side. The percentages of Mn(II) corresponding peaks areas decrease as reaction time increases. While both the percentage of Mn(III) and Mn(IV) corresponding peaks areas increase during this time period. Mn 2p spectra results demonstrate that Mn(II) is mainly adsorbed onto CuO surface within 0.5 hr. As the reaction proceeds, the Mn(II) is gradually oxidized into Mn(III) and Mn(IV). The small difference between Mn 2p XPS and in situ Mn K-edge XAS analyses are attributed to 1) the different sample preparation that in situ XAS spectroscopy measures Mn K-edge in the suspensions, while XPS spectroscopy measures Mn 2p spectra for the freeze-dried solid samples; and 2) the different detection distance of two X-ray techniques that XAS spectroscopy is applied to collect whole bulk Mn speciation and Mn 2p XPS can only collect the information of surface Mn speciation. Appendix A Fig. S5 exhibits the As 3d core level of the CuO surface after As(III) reaction with CuO in the presence of Mn(II) at different time periods. The spectra intensity is stronger at 2 hr than that of at 0.5 hr and there is no shift in peak binding energy, indicating that As(III) adsorption is a predominant reaction within the first 2 hr. As the reaction proceeds, the peak binding energy shifts about 0.5 eV from low energy to high energy at 6 and 12 hr. Binding energy of As 3d core level for As(V) is 1 eV greater than that of As(III) (Liu et al., 2015). The energy shift of As 3d spectra in tested samples indicates that As(III) is gradually oxidized to As(V) on CuO surface.

### 3. Discussion

### 3.1. Mechanisms of CuO-catalyzed Mn(II) oxidation

The Fig. 1 results indicate that Mn(II) oxidation is pH-dependent and the pH-dependent oxidation of Mn(II) is likely related to the redox potential distinctions of Mn-(oxyhydr)oxides/Mn(II) at different pH values (Stumm and Morgan, 2012). The higher the solution pH values are, the smaller the redox potentials are.

Previous studies indicated that the presence of  $\gamma$ -FeOOH,  $\alpha$ -FeOOH, silica, and  $\delta$ -A1<sub>2</sub>O<sub>3</sub> (Davies and Morgan, 1989), hematite (Junta and Hochella Jr, 1994), ferrihydrite (Wang et al., 2015) can promote Mn(II) oxidation, leading to the formation of various Mn(III, IV) oxides. Our results indicate that Mn(II) oxidation is greatly facilitated in the presence of CuO and  $\alpha$ -Fe<sub>2</sub>O<sub>3</sub> under the air atmosphere and O<sub>2</sub> is the oxidant for Mn(II) oxidation. Meanwhile, the catalytic reactivity toward Mn(II) oxidation is different among four metal oxides. The higher catalytic ability of CuO and  $\alpha$ -Fe<sub>2</sub>O<sub>3</sub> than ZnO and  $\gamma$ -Al<sub>2</sub>O<sub>3</sub> at each same pH may probably be attributed to their different performance in electron conductivity. The redox couples of different metals for our experimental metal oxides are summarized in the following Reactions (1)–3 (Li et al., 2012) and

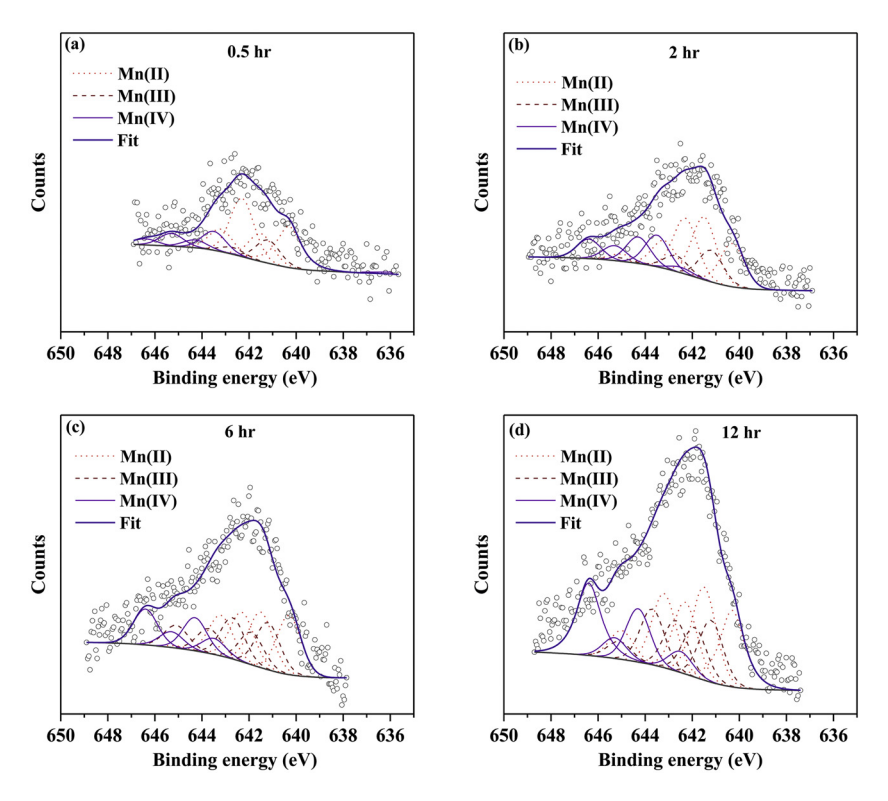


Fig. 6 – High-resolution Mn 2p spectra and fitted data of CuO, Mn(II) and As(III) ternary system after 0.5 hr (a), 2 hr (b), 6 hr (c) and 12 hr (d) reaction with 10 mg/L As(III) under air condition at pH 8. The fitting parameters are shown in Appendix A Table S4.

are highly independent on solution pH levels:

$$\label{eq:Fe2+} \text{Fe}^{2+}/\text{Fe}^{3+}\Big(\text{Fe}^{3+}+\text{e}^{-}\to\text{Fe}^{2+}, \text{E}^{0}=0.77\text{ V}\Big), \tag{1}$$

$$Cu^{+}/Cu^{2+}\Big(Cu^{2+}+e^{-}\to Cu^{+}, E^{0}=0.16\ V\Big), \tag{2}$$

$$Zn^{+}/Zn^{2+} (Zn^{2+} + e^{-} \rightarrow Zn^{+}, E^{0} = 1.04 \text{ V}),$$
 (3)

Al<sub>2</sub>O<sub>3</sub> is not a valence changeable metal oxide and thus cannot be associated to redox reaction, which can always explain the weaker catalytic ability of  $\gamma$ -Al<sub>2</sub>O<sub>3</sub> than CuO and  $\alpha\text{-Fe}_2\text{O}_3.$  Although the redox potential of  $\text{Zn}^+/\text{Zn}^{2+}$  is much greater than those of Fe<sup>2+</sup>/Fe<sup>3+</sup> and Cu<sup>+</sup>/Cu<sup>2+</sup>, ZnO does not displays greater catalytic ability for Mn(II) oxidation when compared to CuO and  $\alpha$ -Fe<sub>2</sub>O<sub>3</sub>. Therefore, the catalytic reactivity cannot be solely attributed to the traditional chemical redox pathway from the redox property of metals. The higher catalytic reactivity of CuO and α-Fe<sub>2</sub>O<sub>3</sub> than Al<sub>2</sub>O<sub>3</sub> and ZnO for Mn(II) oxidation can be attributed to three possible pathways: 1) the direct electron transfer (ET) from Mn(II) to O2 [ET in Mn(II)-O2]; 2) electron transfer from the adsorbed Mn(II) complex on mineral surface to O2 [ET in metal oxide-Mn(II)-O2]; and 3) indirect electron transfer from Mn(II) passing through metal oxides to O2 bridged by the metal oxides [ET in the Mn(II)-metal oxide-O2 complexes]. The detailed description of these three possible pathways can be found in Appendix A Text S3.

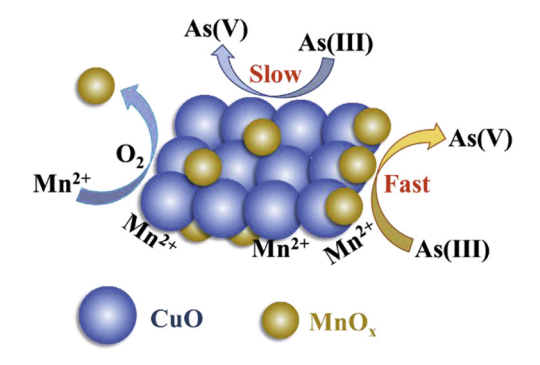


Fig. 7 – A mechanistic scheme of simultaneous Mn(II) and As(III) oxidation on CuO surface at circumneutral pHs.

### 3.2. Role of Mn(II) on As(III) adsorption and oxidation

A previous study showed that Mn(II) oxidation on ferrihydrite surface promoted the As(III) oxidation (Lan et al., 2018). The similar effect from Mn(II) is observed at the surface of CuO in this study. Batch experiment results indicate that  $O_2$  is the final electron acceptor for As(III) oxidation in the presence of Mn(II) (Fig. 7). Mn(II) can be oxidized on the surface of CuO to Mn(III) and Mn(IV) phases by  $O_2$  in the air. Both Mn(III) and Mn(IV) species may be responsible for As(III) oxidation.

To identify the potential production of Mn(III) and Mn(IV) oxides generated on the surface of CuO, TEM image and EDS

spectra have been applied to reveal the morphology of newly formed MnOx on CuO. TEM image do not show any alternation of CuO morphology before and after the reaction (Appendix A Fig. S6) and the formation of any new phases, corresponding to MnO<sub>x</sub> solid phases. TEM image of raw unreacted CuO could be found in our previous study (Zeng et al., 2018). The XRD characterization was also collected to reveal the formation of new Mn oxide phases. The XRD patterns do not show the presence of any MnOx phases and only CuO diffraction patterns have been observed (data not shown), probably since the portion of newly formed MnOx (only 0.78 mmol/L Mn(II) added in this study) was too low and its XRD reflection was below the detection limitation of XRD (Jung et al., 2021b). However, our in situ Mn K-edge XAS and Mn 2p XPS show the formation of highvalent Mn(III) and Mn(IV), and that the dominant Mn species is Mn(III), which has a high reactivity to promote As(III) oxidation at circumneutral pHs (Figs. 5 and 6, Table 2 and Appendix A Table S3).

Additionally, combined XPS and XAS spectroscopic results indicate that in the presence of As(III), Mn(III) produced from Mn(II) oxidation is likely reduced back to Mn(II) for the As(III) oxidation and Mn(II) oxidation into Mn(III) proceeds after As(III) is completely oxidized to As(V). Our previous study indicated that CuO could rapidly catalyze the oxidation of As(III) at alkaline pHs (e.g., pH 11) and has an obvious shortage when applied to As(III) oxidation at circumneutral pHs (e.g., pH 8) and the oxidation extent is low at pH 8 (Zeng et al., 2018). In this study, we propose that Mn(II) plays a critical role as an electron shuttle, which can significantly promote the rapid oxidation of As(III) at circumneutral pH (Fig. 7).

Even though the presence of Mn(II) significantly facilitates As(III) oxidation, the impacts of Mn(II) on As(III) and As(V) adsorption during As(III) oxidation also need to evaluate for the application of CuO usage in As(III) removal. According to the previous study, in the Fe-Mn binary oxide system, Mn(II) oxidation on metal oxide surface decreases the adsorption of initial As(III) and produced As(V) probably due to the sites of Fe oxide surface being occupied by the produced Mn(III) and Mn(IV) oxides (Zhang et al., 2014a). With high PZC of 9.2 and large SSA of 79.03 m<sup>2</sup>/g, CuO has a strong ability of As adsorption at pH 8 (Zeng et al., 2018). The Mn(II) promotion for As oxidation and adsorption could be attributed to a higher adsorption affinity of oxide materials for As(V) than As(III) at pH 8 since As(V) has higher ionization magnitude than As(III) (Goldberg, 2002). Mn(II) might enhance As(V) co-adsorption on CuO via forming surface ternary complexes of CuO surface-Mn(II)-As(V) since Mn(II) and As(V) have oppositive charge at our study pH or due to modification of surface electrostatic interactions (Yan et al., 2022). In addition, oxidation of As(III) in the presence of Mn(II) was promoted on the ferrihydrite surface by the pumping of O2 (Lan et al., 2018). However, in our study, high As(III) oxidation rate can be achieved under air atmosphere without extra O2 pumping in the CuO, Mn(II), and As(III) ternary system (Fig. 4 and Table 1), which might be an obvious advantage for its engineering application. At pH 8, the catalyzed activity of CuO toward Mn(II) and As(III) oxidation are comparable with α-Fe<sub>2</sub>O<sub>3</sub>, which also displays high promotive effect on Mn(II) catalyzed oxidation as CuO does (Figs. 1 and 2).

However,  $\alpha\text{-Fe}_2O_3$  is not the main focus of this study and the related research of Fe oxide-catalyzed Mn(II) and As(III) oxidation should be warranted in the future to explore the influences of Fe oxides' surface properties and crystalline structures. Finally, the mechanistic investigations of metal oxide-catalyzed simultaneous Mn(II) and As(III) oxidation are expected to give practical and theoretical guidance on the potential application of CuO for the remediation of Mn(II) and As(III) contamination.

#### 4. Conclusions

In this work, Mn(II) oxidation on a variety of common metal oxides (CuO,  $\alpha$ -Fe<sub>2</sub>O<sub>3</sub>,  $\gamma$ -Al<sub>2</sub>O<sub>3</sub> and ZnO) and simultaneous oxidation and removal of Mn(II) and As(III) on CuO surface were studied. Our results indicate that CuO can rapidly catalyze the oxidation of Mn(II) and As(III) into low toxic components. O2 is the terminal electron acceptor of Mn(II) and As(III) oxidation on CuO surface and Mn(II) can act as an electron shuttle to promote As(III) oxidation and removal. The oxidized product of Mn(II) in the presence of CuO is mainly as highvalent MnOx phases. This newly formed Mn(III) and Mn(IV) species can promote As(III) oxidation by CuO at circumneutral pH 8. This study broadens our current understanding of both adsorption and oxidation catalytic reactivity of engineering metal oxides and provides new insights for the mechanisms of aqueous Mn(II) and As(III) simultaneous oxidation on CuO surface at near-neutral pHs.

### Acknowledgments

This work is supported by the National Natural Science Foundation of China (Nos. 42030709, 42167031), the National Key Research and Development Program of China (No. 2017YFD0200201). Y.T. acknowledges support by the U.S. National Science Foundation (NSF) under Grant No. 2108688. We thank Dr. Rixiang Huang for the valuable suggestions during manuscript writing.

#### Appendix A Supplementary data

Supplementary material associated with this article can be found, in the online version, at doi:10.1016/j.jes.2022.03.031.

#### REFERENCES

Bargar, J.R., Tebo, B.M., Bergmann, U., Webb, S.M., Glatzel, P., Chiu, V.Q., et al., 2005. Biotic and abiotic products of Mn (II) oxidation by spores of the marine Bacillus sp. strain SG-1. Am. Mineral. 90, 143–154.

Bissen, M., Frimmel, F.H., 2003. Arsenic-a review. Part II: Oxidation of arsenic and its removal in water treatment. Acta Hydroch. Hydrob. 31, 97–107.

Butterfield, C.N., Soldatova, A.V., Lee, S.W., Spiro, T.G., Tebo, B.M., 2013. Mn(II, III) oxidation and  $MnO_2$  mineralization by an expressed bacterial multicopper oxidase. P. Natl Acad. Sci. USA 110, 11731–11735.

- Cao, A.M., Monnell, J.D., Matranga, C., Wu, J.M., Cao, L.I., Gao, D., 2007. Hierarchical nanostructured copper oxide and its application in arsenic removal. J. Phys. Chem. C 111, 18624–18628.
- Clement, B.G., Luther III, G.W., Tebo, B.M., 2009. Rapid, oxygen-dependent microbial Mn (II) oxidation kinetics at sub-micromolar oxygen concentrations in the Black Sea suboxic zone. Geochim. Cosmochim. Ac. 73, 1878–1889.
- Coddington, K., 1986. A review of arsenicals in biology. Toxicol. Environ. Chem. 11, 281–290.
- Davies, S.H., Morgan, J.J., 1989. Manganese (II) oxidation kinetics on metal oxide surfaces. J. Colloid Interf. Sci. 129, 63–77.
- Emerson, D., 2000. Microbial oxidation of Fe (II) and Mn (II) at circumneutral pH. In: Lovley, R.D. (Ed.), Environmental Microbe-Metal Interactions. ASM Press, pp. 31–52.
- Ferguson, J.F., Gavis, J., 1972. A review of the arsenic cycle in natural waters. Water Res 6, 1259–1274.
- Ginder-Vogel, M., Landrot, G., Fischel, J.S., Sparks, D.L., 2009. Quantification of rapid environmental redox processes with quick-scanning X-ray absorption spectroscopy (Q-XAS). P. Natl Acad. Sci. USA 106, 16124–16128.
- Goldberg, S., 2002. Competitive adsorption of arsenate and arsenite on oxides and clay minerals. Soil Sci. Soc. Am. J. 66, 413–421.
- Jung, H., Snyder, C., Xu, W., Wen, K., Zhu, M., Li, Y., Lu, A., Tang, Y., 2021a. Photocatalytic oxidation of dissolved  $\mathrm{Mn^{2+}}$  by  $\mathrm{TiO_2}$  and the formation of tunnel structured manganese oxides. ACS Earth Space Chem 5, 105–2114.
- Jung, H., Xu, X., Wan, B., Wang, Q., Borkiewicz, O.J., Li, Y., Chen, H., Lu, A., Tang, Y., 2021b. Photocatalytic oxidation of dissolved Mn (II) on natural iron oxide minerals. Geochim. Cosmochim. Ac. 312, 343–356.
- Junta, J.L., Hochella Jr., M.F., 1994. Manganese (II) oxidation at mineral surfaces: A microscopic and spectroscopic study. Geochim. Cosmochim. Ac. 58, 4985–4999.
- Katsoyiannis, I.A., Zouboulis, A.I., 2006. Use of iron-and manganese-oxidizing bacteria for the combined removal of iron, manganese and arsenic from contaminated groundwater. Water Qual. Res. J. 41, 117–129.
- Lan, S., Ying, H., Wang, X., Liu, F., Tan, W., Huang, Q., et al., 2018. Efficient catalytic As (III) oxidation on the surface of ferrihydrite in the presence of aqueous Mn (II). Water Res 128, 92–101.
- Li, Y., Zhang, W., Niu, J., Chen, Y., 2012. Mechanism of photogenerated reactive oxygen species and correlation with the antibacterial properties of engineered metal-oxide nanoparticles. ACS Nano 6, 5164–5173.
- Liu, C.H., Chuang, Y.H., Chen, T.Y., Tian, Y., Li, H., Wang, M.K., et al., 2015. Mechanism of arsenic adsorption on magnetite nanoparticles from water: Thermodynamic and spectroscopic studies. Environ. Sci. Tech. 49, 7726–7734.
- Madden, A.S., Hochella Jr., M.F., 2005. A test of geochemical reactivity as a function of mineral size: Manganese oxidation promoted by hematite nanoparticles. Geochim. Cosmochim. Ac. 69, 389–398.
- Manceau, A., Marcus, M.A., Grangeon, S., 2012. Determination of Mn valence states in mixed-valent manganates by XANES spectroscopy. Am. Mineral. 97, 816–827.

- Manning, B.A., Fendorf, S.E., Bostick, B., Suarez, D.L., 2002. Arsenic (III) oxidation and arsenic (V) adsorption reactions on synthetic birnessite. Environ. Sci. Tech. 36, 976–981.
- Martinson, C.A., Reddy, K., 2009. Adsorption of arsenic (III) and arsenic (V) by cupric oxide nanoparticles. J. Colloid Interf. Sci. 336. 406–411.
- McDonald, K.J., Reynolds, B., Reddy, K., 2015. Intrinsic properties of cupric oxide nanoparticles enable effective filtration of arsenic from water. Sci. Rep. 5, 1–10.
- Ren, H.T., Jing, M.Z., Liang, Y., Li, T.T., Jiang, S.M., Lou, C.W., et al., 2021. Performance and mechanism involved in the cascade oxidation of Mn (II) and As (III) by Bi<sub>2.15</sub>WO<sub>6</sub> under alkaline conditions. J. Environ. Chem. Eng. 9, 106196.
- Schaefer, M.V., Plaganas, M., Abernathy, M.J., Aiken, M.L., Garniwan, A., Lee, I., et al., 2020. Manganese, arsenic, and carbonate interactions in model oxic groundwater systems. Environ. Sci. Tech. 54, 10621–10629.
- Stumm, W., Morgan, J.J., 2012. Aquatic chemistry: Chemical equilibria and rates in natural waters. John Wiley & Sons.
- Wang, X., Lan, S., Zhu, M., Ginder-Vogel, M., Yin, H., Liu, F., et al., 2015. The presence of ferrihydrite promotes abiotic formation of manganese (oxyhydr) oxides. Soil Sci. Soc. Am. J. 79, 1297–1305
- Webb, S.M., Dick, G.J., Bargar, J.R., Tebo, B.M., 2005. Evidence for the presence of Mn (III) intermediates in the bacterial oxidation of Mn (II). P. Natl Acad. Sci. USA 102, 5558–5563.
- Yan, Y., Wan, B., Mansor, M., Wang, X., Zhang, Q., Kappler, A., et al., 2022. Co-sorption of metal ions and inorganic anions/organic ligands on environmental minerals: A review. Sci. Total Environ. 803, 149918.
- Yin, H., Liu, F., Feng, X., Hu, T., Zheng, L., Qiu, G., et al., 2013. Effects of Fe doping on the structures and properties of hexagonal birnessites: comparison with Co and Ni doping. Geochim. Cosmochim. Ac. 117, 1–15.
- Yu, X.Y., Xu, R.X., Gao, C., Luo, T., Jia, Y., Liu, J.H., et al., 2012. Novel 3D hierarchical cotton-candy-like CuO: Surfactant-free solvothermal synthesis and application in As (III) removal. ACS Appl. Mater. Interf. 4, 1954–1962.
- Zeng, L., Wan, B., Huang, R., Yan, Y., Wang, X., Tan, W., et al., 2018. Catalytic oxidation of arsenite and reaction pathways on the surface of CuO nanoparticles at a wide range of pHs. Geochem. Trans. 19, 1–12.
- Zhang, G., Liu, F., Liu, H., Qu, J., Liu, R., 2014a. Respective role of Fe and Mn oxide contents for arsenic sorption in iron and manganese binary oxide: An X-ray absorption spectroscopy investigation. Environ. Sci. Tech. 48, 10316–10322.
- Zhang, Q., Zhang, K., Xu, D., Yang, G., Huang, H., Nie, F., Liu, C., Yang, S., 2014b. CuO nanostructures: Synthesis, characterization, growth mechanisms, fundamental properties, and applications. Prog. Mater. Sci. 60, 208–337.
- Zhu, Y., Liang, X., Zhao, H., Yin, H., Liu, M., Liu, F., et al., 2017. Rapid determination of the Mn average oxidation state of Mn oxides with a novel two-step colorimetric method. Anal. Methods 9, 103–109.